Earthquake Geotechnical Engineering for Protection and Development of Environment and Constructions – Silvestri & Moraci (Eds)
© 2019 Associazione Geotecnica Italiana, Rome, Italy, ISBN 978-0-367-14328-2

Analysis of seismic earth pressures on flexible underground box structures

M.G. Durante
University of Texas, Austin, TX, USA

S.J. Brandenberg
University of California, Los Angeles, CA, USA

S. Dashti
University of Colorado, Boulder, CO, USA

J.P. Stewart
University of California, Los Angeles, CA, USA

G. Mylonakis
University of Bristol, Bristol, UK

ABSTRACT: The seismic response of underground structures is controlled by a combination of kinematic and inertial soil-structure interaction. Kinematic interaction arises from differences in the displaced shape of the underground structure relative to the free-field soil, while inertial interaction arises from mass being accelerated by earthquake ground motion. Kinematic interaction is typically the dominant source of SSI for underground structures, though inertial interaction could be significant when above ground structural components are attached to the walls. This paper presents kinematic Winkler based analytical solutions of a centrifuge testing program involving an underground box structure bolted to the base of the model container and embedded in dry sand. The model was shaken by a sequence of earthquake ground motions. Input parameters include (*i*) the free-field soil profile (shear wave velocity and mass density), (*ii*) the flexural stiffness of the wall, (*iii*) rotational and translational stiffnesses at the base and top of the wall, and (*iv*) the ground surface motion. The soil stiffness is assumed to vary with depth according to a power law. The measured surface motion is deconvolved in the frequency domain to obtain depth-dependent displacements that are compatible with the soil profile, and these displacements are utilized as inputs to the Winkler model. The soil stiffness is set to be compatible with mobilized free-field strain levels in accordance with a modulus reduction and damping curve (i.e., the analysis is equivalent-linear). Results are presented in terms of the measured versus predicted earth pressure distributions mobilized at the soil-wall interface and the bending strains mobilized in the wall. Standard of practice procedures in which an inertial force is imposed on an active wedge are also performed. Agreement between measured and predicted quantities is significantly better for the kinematic SSI analytical solution than for standard of practice procedures.

1 INTRODUCTION

The seismic response of underground structures can be studied using soil-structure interaction (SSI) principals, assuming that the response of the system is a combination of kinematic and inertial interaction. Kinematic interaction arises from differences in the displaced shape of the underground structure relative to the free-field soil, while inertial interaction arises from mass being accelerated by earthquake ground motion. Typically, kinematic interaction is the

dominant source of SSI for shallow underground structures, unless structural components are attached to or adjacent the walls, generating significant inertial interaction.

The seismic response of underground structures is traditionally analyzed using limit equilibrium methods based on the effect of an inertial force imposed on an active wedge, known as the Mononobe- Okabe (M-O) approach (Okabe 1924, Mononobe & Matsuo 1929) with subsequent variations by Seed and Whitman (1970). Important limitations of the M-O approach are: (*i*) failure to consider the wavelength of the free-field ground motion, (*ii*) the inability to model flexibility of the wall elements, and (*iii*) the inability to model seismic earth pressures for loading cases that do not produce a condition of limiting equilibrium. An alternative to these limit analysis procedures is provided by elasto-dynamic solutions, usually based on a vertically propagating shear wave acting on a vertical rigid wall (Wood 1973, Arias et al. 1981, Veletsos & Younan 1994, Younan & Veletsos 2000, Ostadan 2005, Papazafeiropoulos & Psarropoulos 2010, Kloukinas et al. 2012, and Vrettos et al 2016). A limitation of elasto-dynamic solutions is the assumption that the soil rests atop a rigid base layer, which produces strong resonances that are unrealistic for real systems. Brandenberg et al. (2015) developed an elasto-dynamic Winkler based framework for solving the kinematic wall-soil interaction problem for deeper soil conditions. Their model assumed: (*i*) a uniform soil shear modulus with depth, (*ii*) rigid walls, (*iii*) lack of gapping at the soil-wall interface, and (*iv*) elastic soil behavior. Brandenberg et al. (2017) subsequently developed a solution for Winkler stiffness intensity for vertically inhomogeneous soils, which is a more accurate representation of the properties of most retained soils.

In this paper, a kinematic Winkler based analytical solution is used to model results from a centrifuge testing program including one simplistic experiment where an underground box structure representing a buried reservoir structure was bolted to the base of the container and embedded in medium-dense, dry Nevada sand (Hushmand et al. 2016a, b, and c). Results are presented in terms of measured versus predicted seismic earth pressure distributions mobilized at the soil-wall interface and the seismic bending strains mobilized in the wall. Results from the most commonly used M-O approaches are also presented as a point of comparison. The comparison shows that the kinematic solution is more accurate than the M-O methods.

2 ANALYTICAL PROCEDURE

Kinematic seismic earth pressure on flexible underground structures can be evaluated by means of a Winkler model, based on an approximate elasto-dynamic solution obtained from the governing equation reported in Equation 1, computed per unit width under the plane strain assumption.

$$EI \cdot u^{(4)}(z) + k^{i}_{yH} f(z)\big(u(z) - u_g(z)\big) = 0 \tag{1}$$

where EI is flexural stiffness of the wall (assumed constant), $u^{(4)}(z)$ represents the fourth derivative of the wall displacement with respect to the depth ($z = 0$ at surface), k^{i}_{yH} is the Winkler stiffness intensity (measured in units of force per length cubed) at the base of the wall, u_g represents the free-field displacement, and $f(z)$ is a dimensionless function that represents the variation of Winkler stiffness intensity with depth.

The shear waves are assumed to propagate vertically in an inhomogeneous soil deposit assuming the function of depth proposed by Rovithis et al. (2011), as defined in Equations 2-3, where G is the shear modulus, ρ is the mass density, V_0 is the shear wave velocity at the surface, V_r is the shear wave velocity at the base of the soil layer, n is an inhomogeneity factor, and $b=(V_0/V_r)^{1/n}$. Note that $n = 0$ corresponds to homogeneous soil (e.g. over-consolidated clay), and $n = 0.5$ corresponds to a linear variation in shear modulus with depth (which can model normally consolidated clay). Mass density (ρ) and Poisson's ratio (υ) are assumed constant within the soil deposit. The measured surface motion is used as input parameter in the analysis and it is used to compute the mobilized free-field strain levels in accordance with a modulus reduction and damping curve (i.e., the analysis is equivalent-linear). The soil stiffness is then set to be compatible with the computed modulus reduction and damping values and

the measured ground motion is deconvolved in the frequency domain to obtain depth-dependent displacements that are compatible with the inhomogeneous soil profile (Rovithis et al. 2011). These displacements are then used as input to the Winkler model.

$$G(z) = \rho \; V_r^2 \cdot f(z) \tag{2}$$

$$f(z) = \left[b + (1-b)\frac{z}{z_r} \right]^{2n} \tag{3}$$

The Winkler stiffness intensity at the base of the wall $k^i{}_{yH}$ is computed using Equation 4, where $k^i{}_{yH0}$ is the static Winkler stiffness intensity at the base of the rigid wall (Equation 5), and ζ_{freq}, ζ_{length}, and ζ_{flex}, are scalar adjustment factors to account for frequency, finite deposit length, and wall flexibility, respectively. $k^i{}_{yH0}$, ζ_{freq}, and ζ_{length} are based on the solution by Brandenberg et al. (2017), while ζ_{flex} is based on continuum finite element solutions of flexible walls retaining inhomogeneous soils (Durante et al. 2018). The values of ζ_{freq} and ζ_{length} depend on dimensionless frequency, a_o (Eq. 7), the dimensionless first-mode frequency of a finite-length deposit $\hat{a}_{oc}$, which in turn depends on the dimensionless first mode frequency of an infinite-length deposit, a_{oc}, and a stiffness multiplier, b_{oc}, that arises from soil inhomogeneity. The flexibility of the wall is defined relatively to the soil using a dimensionless constant βH, where β is defined by Equation 14. The flexibility of the wall relative to the soil increases with βH and the wall is essentially rigid for βH smaller than 0.5.

$$k^i_{yH} = k^i_{yH0} \cdot \zeta_{freq} \cdot \zeta_{length} \cdot \zeta_{flex} \tag{4}$$

where:

$$k^i_{yH0} = \frac{G_H}{H} \frac{2}{\sqrt{(1-\nu)(2-\nu)}} \left[1.057 e^{-1.968(1-n)-3.008b} + \frac{\pi}{2} \right] \tag{5}$$

$$\zeta_{freq} = \sqrt{1 - \frac{a_o^2}{\hat{a}_{oc}{}^2}} \tag{6}$$

$$a_o = \frac{\omega H}{V_H} \tag{7}$$

$$\hat{a}_{oc} = \sqrt{\frac{\frac{2}{1-\upsilon} \; \frac{a_{oc}}{b_{oc}\psi_e} \left(\sinh\left(\frac{L}{H} \; \frac{a_{oc}b_{oc}}{\psi_e} \right) - \frac{L}{H} \; \frac{a_{oc}b_{oc}}{\psi_e} \right)}{\left(2\frac{L}{H} - 3\frac{\psi_e}{a_{oc}b_{oc}} \; \sinh\left(\frac{L}{H} \; \frac{a_{oc}b_{oc}}{\psi_e} \right) + \frac{L}{H} \; \cosh\left(\frac{L}{H} \; \frac{a_{oc}b_{oc}}{\psi_e} \right) \right)} + a_{oc}^2} \tag{8}$$

$$a_{oc} = \frac{\pi}{2} - 0.406 e^{-1.947(1-2n)-2.110b} \tag{9}$$

$$b_{oc} = 1 + 1.172 e^{-2.161(1-2n)-2.974b} \tag{10}$$

$$\psi_e = \sqrt{\frac{(2-\nu)}{(1-\nu)}} \tag{11}$$

$$\zeta_{length} = \frac{1 + exp\left(-\frac{1}{\psi_e b_{oc}\sqrt{a_{oc}^2 - a_o^2}} \; \frac{L}{H} \right)}{\left[1 - exp\left(-\frac{1}{\psi_e b_{oc}\sqrt{a_{oc}^2 - a_o^2}} \; \frac{y_{ref}}{H} \right) + exp\left(-\frac{1}{\psi_e b_{oc}\sqrt{a_{oc}^2 - a_o^2}} \; \frac{L}{H} \right) - exp\left(-\frac{1}{\psi_e b_{oc}\sqrt{a_{oc}^2 - a_o^2}} \; \frac{L - y_{ref}}{H} \right) \right]} \tag{12}$$

$$\zeta_{flex} = 1 + exp\left[1 + \frac{-5.30 + 3.29nb^{2n} + 0.42b^{2n} - 2.52n}{\beta H}\right] \tag{13}$$

$$\beta = \sqrt[4]{\frac{k^i_{yH0}}{4EI}} \tag{14}$$

3 CENTRIFUGE TESTING LAYOUT

3.1 *Model details*

The centrifuge model represents a prototype of a buried water reservoirs being built by the Los Angeles Department of Water and Power, and consists of a rectangular steel box structure (Figure 1). More details about the model can be found in Hushmand et al. (2016a, b, and c). The model was tested on the 5.5 m-radius, 400g-ton geotechnical centrifuge at the University of Colorado Boulder. The structure was bolted to the base of a flexible shear beam container, and dry Nevada sand No. 120 was placed at a relative density of D_r = 60% between the box structure and the container walls. The soil thickness and structure height were both 10.5m in prototype scale (prototype units are used throughout this paper). The structure was composed of steel, and had a base thickness of 0.69m, roof thickness of 0.37m, and wall thickness of 0.56m. This structure can be considered flexible compared to the soil, in fact the dimensionless parameter βH varied in the range 1.5 – 1.9 depending on the level of shaking. Assuming that the shear beam container provides harmonic boundary conditions (e.g., an infinite sequence of identical models connected to each other in series from left-to-right), the centrifuge model represents a finite length soil deposit with the length of the retained soil deposit equal to twice the distance from the container wall to the structure wall, such that L = 29.8m. The model was equipped with accelerometers (A), linearly-variable differential transformers ($LVDTs$ - D), strain gauges (SG), and tactile pressure transducers (TP) that were used to measure the seismic response of the soil-structure system. Furthermore, sensor A9 was utilized as the input motion, and the horizontal distance from A9 to the structure is 11.1m.

3.2 *Ground motions*

Broadband ground motions were applied to the container base in flight by means of a 1D servo-hydraulic shake table (Ketcham et al. 1991). The scaled earthquake motions were selected from the 1994 Northridge, 1999 Izmit, and 1989 Loma Prieta Earthquakes. The Northridge motion was scaled at three different shaking intensities (low, medium, and high). A summary of the ground motion properties achieved in the tests is reported in Table 1 in terms of Peak Ground Acceleration (PGA), Peak Ground Velocity (PGV), Arias Intensity (I_a), significant duration ($D_{5\text{-}95}$), and mean period (T_m).

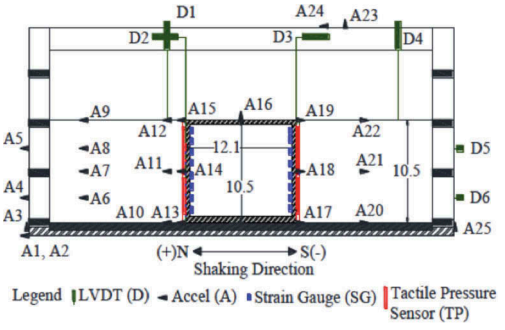

Figure 1. Elevation view of centrifuge - dimensions shown in prototype scale meters (Hushmand et al. 2016c).

Table 1. Scaled ground motions properties (**M**=Moment magnitude).

Event	Station	Test ID	PGA (g)	PGV (m/s)	I_a (m/s)	$D_{5\text{-}95}$ (s)	T_m (s)
1994 Northridge Earthquake (**M** 6.7)	Sylmar Converter Station	Northridge-L	0.55	0.44	1.99	17.96	0.44
		Northridge-M	0.46	0.36	8.88	19.88	0.56
		Northridge-H	0.64	0.55	18.27	25.99	0.56
1999 Izmit Earthquake (**M** 7.6)	Istanbul Station	Izmit	1.08	0.74	3.39	39.42	0.63
1989 Loma Prieta Earthquake (**M** 6.9)	LGPC Station	Loma Prieta	1.24	0.85	22.07	14.13	0.50

Table 2. Estimated soil properties and βH prior to each motion in the centrifuge.

Test ID	PGV (m/s)	f_0 (Hz)	V_h (m/s)	γ_{ref} (%)	G/G_{max}	D (%)	βH
Northridge-L	0.44	4.2	140	0.11	0.49	11.0	1.5
Northridge-M	0.36	6.0	200	0.11	0.50	10.8	1.8
Northridge-H	0.55	6.0	200	0.20	0.31	15.4	1.6
Izmit	0.74	6.0	200	0.06	0.67	7.7	1.9
Loma Prieta	0.85	6.6	220	0.18	0.33	14.5	1.7

3.3 *Soil properties*

In order to account for soil densification caused by shaking, the shear wave velocity profile was computed prior to each motion based on the first frequency of the deposit (f_0) obtained from centrifuge ambient vibrations. In particular, f_0 was used to define the shear wave velocity at the base of the deposit (V_H) assuming an inhomogeneous soil deposit with n=0.25 and b=0.01. Taking into account that the centrifuge model is not able to reproduce free-field conditions, a 2D correction was used to compute V_H, as suggested in Brandenberg et al. 2017.

The measured surface motion (u_{g0}) was then used to compute the representative uniform mobilized free-field strain level for the deposit (γ_{ref}, Idriss & Sun 1991, Equation 5) in accordance with modulus reduction and damping curves proposed by Elgamal et al. 2005. Base displacement in Equation 6 (u_{gH}) was computed from the deconvolution in the frequency domain of the surface motion (Rovithis et al. 2011). Several iterations were necessary to find the mobilized free-field strain level. Table 2 shows the soil properties obtained for the selected ground motions.

$$\gamma_{ref} = \gamma_{av} \cdot \frac{M-1}{10} \tag{5}$$

where $\boldsymbol{M}$ is the magnitude of the ground motion and:

$$\gamma_{av} = max\left(\frac{u_{g0} - u_{gH}}{H}\right) \tag{6}$$

4 COMPARISON OF RESULTS

Figure 2 shows the comparison of the analytical solution with the experimental centrifuge test results in terms of snapshots of maximum increment of seismic earth pressure ($\Delta\sigma_{xx}$) and maximum increment of bending strain ($\mu\varepsilon$) acting on the wall versus depth at the time of the maximum bending strain. The predicted bending strains are in good agreement with the experimental data for the Northridge-L, Izmit, and Loma Prieta motions, and under-predict the response for the Northridge-M and Northridge-H motions. On the contrary, a mismatch between the predicted and measured increment of seismic earth pressure is observed. These

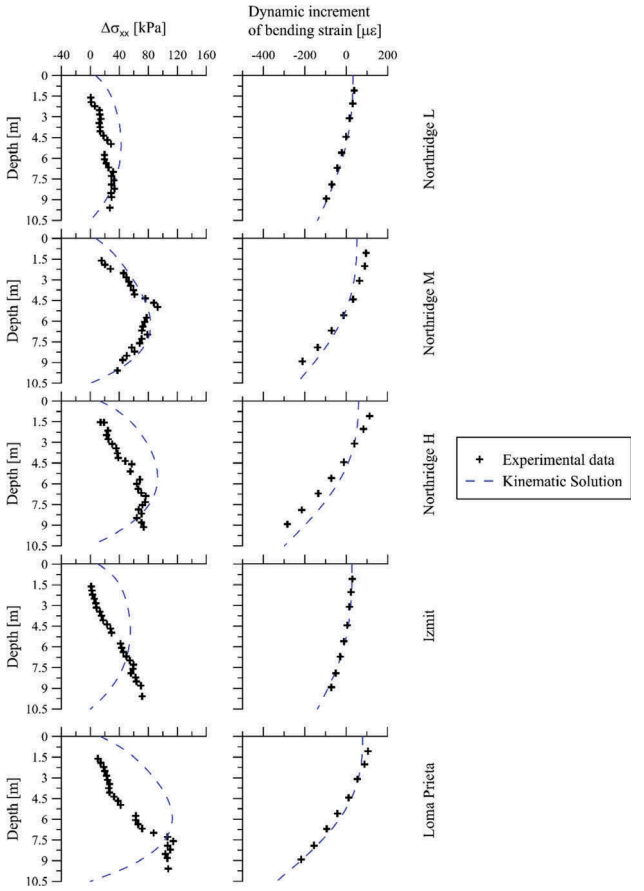

Figure 2. Comparison kinematic analytical solution with experimental centrifuge data (Hushmand et al. 2016) in terms of maximum increment of seismic earth pressure ($\Delta\sigma_{xx}$) and maximum increment of bending strain ($\mu\varepsilon$) acting on the wall versus depth.

observations are consistent with prior comparisons between nonlinear finite element soil-structure interaction simulations and the same centrifuge experiments (e.g., Deng et al. 2016). This response may have been influenced by the following aspects: (*i*) the accuracy of the tactile pressure transducers is expected to be worse than the accuracy of strain gauges and other sensors used in centrifuge (e.g., see Gillis et al. 2015); (*ii*) the tactile pressure transducers and strain gauges were recorded with different data acquisition systems, and pressures are reported at the time of maximum resultant seismic thrust rather than at the time of peak bending strain, and (iii) the Winkler solution is known to predict earth pressure distributions that are shifted up, with the resultant acting too high on the wall (e.g., Brandenberg et al. 2017).

Figure 3 shows the discrepancy between the measured bending strain and the predicted values at the elevation closest to the base of the wall versus the surface far-field motion PGV (Figure 3a) and the measured maximum average shear strain (Figure 3b) for the earthquake ground motions considered. Three solutions based on the M-O approach are reported in the plot. The M-O values were obtained considering a soil friction angle of 35° (Hushmand et al. 2016c) and a triangular seismic pressure increment along the wall, with centroid at 1/3 of the height of the wall. Three different values of Peak Ground Acceleration (PGA) were used: (*i*) the full soil surface (PGA), (*ii*) 65% of PGA, and (*iii*) the average PGA acting over the height of the wall (Wagner & Sitar, 2016). Figure 3 shows that the kinematic analytical solution produces peak bending strain estimates with errors in the range of about -32% to +13%, while the M-O solutions range from -70% to +∞. The kinematic solution is accurate for the smaller motions and tends to under-predict

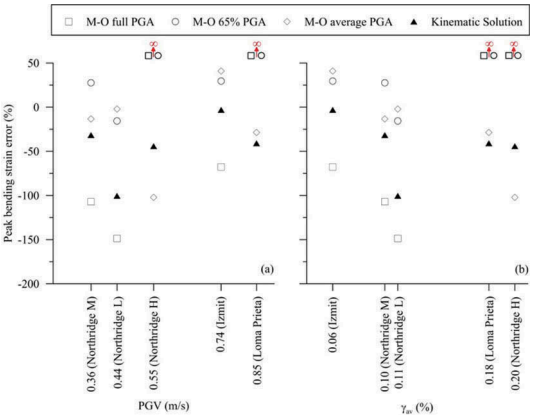

Figure 3. Discrepancy between models and experimental data versus (a) surface far-field motion PGV and (b) maximum average shear strain (γ_{av}).

the response as the motion PGV and induced strain values become larger. This is likely due to the limitations of an equivalent linear approach for strong motions, and perhaps also the increased role of inertial SSI effects as the soil softens. The M-O solutions approach ∞ when the level of ground shaking becomes large enough to fail the retained soil along a plane parallel to the ground surface. Strictly speaking, the M-O approach does not provide a physically meaningful solution at higher levels of ground shaking, and we interpret earth pressures to be ∞ for this condition despite the lack of a mathematical solution. The analytical solution is not limited by the level of shaking, and would only predict infinite earth pressure in the case when the shaking level is also infinite.

Causes for error in the kinematic solutions are likely due to (*i*) limitations of the equivalent linear analysis method, particularly for strong shaking events that mobilized significant non-linear and plastic soil response, (*ii*) limitations of the Winkler assumption, which is known to differ from more robust continuum solutions, and (*iii*) lack of consideration of inertial interaction, which may not be negligible due to the presence of the roof diaphragm, particularly at stronger levels of shaking. Despite these limitations, the kinematic solutions are nevertheless more accurate than the M-O solutions.

5 CONCLUSIONS

Seismic earth pressures on a flexible underground box structure has been analyzed in this paper using a soil-structure interaction approach. In particular, the kinematic interaction has been evaluated using a Winkler based analytical solution that considers the relative displacement between soil and structure. The analytical solution has been validated using the results of a centrifuge test involving a flexible and unyielding underground box structure bolted to the base of the container and embedded in medium-dense, dry sand. Results have been presented in terms of the measured versus predicted earth pressure distributions mobilized at the soil-wall interface and the bending strains mobilized in the wall. Agreement between measured and predicted peak bending strains was good for three motions, while under-prediction was observed for two motions. By contrast, predicted earth pressure distributions differed more significantly from measurements. Despite its limitations, the kinematic SSI procedure was more accurate than standard of practice procedures based on the Mononobe-Okabe approach for this particular class of shallow underground box structures.

REFERENCES

Arias A., Sanchez-Sesma F.J., Ovando-Shelley E. 1981. A simplified elastic model for seismic analysis of earth-retaining structures with limited displacements. In *Proceedings of the International Conference on*

Recent Advances in Geotechnical Earthquake Engineering *and* Soil Dynamics, St. Louis, Mo., Vol. 1, pp. 235–240.

Brandenberg S.J., Mylonakis G., Stewart J.P. 2015. Kinematic framework for evaluating seismic earth pressures on retaining walls. *Journal of Geotechnical and Geoenvironmental Engineering*; 141(7),1–10.

Brandenberg, S.J., Mylonakis G., Stewart J.P. 2017. Approximate solution for seismic earth pressures on rigid walls retaining inhomogeneous elastic soil. *Soil Dynamics and Earthquake Engineering*; 97:468–477.

Deng Y.H., Dashti S., Hushmand A., Davis C., Hushmand B. 2016. Seismic Response of Underground Reservoir Structures in Sand: Evaluation of Numerical Simulations using Centrifuge Experiments. *Soil Dynamics and Earthquake Engineering*; 85, 202–216.

Durante M. G., Brandenberg S. J., Stewart J. P., Mylonakis G. 2018. Winkler stiffness intensity for flexible walls retaining inhomogeneous soil. *5th Geotechnical Earthquake Engineering and Soil Dynamics Conference (GEESD2018)*, June 10-13 2018, Austin, Texas.

Elgamal, A., Yang, Z., Lai, T., Kutter, B. L., Wilson, D. W. 2005. Dynamic Response of Saturated Dense Sand in Laminated Centrifuge Container. *Journal of Geotechnical and Geoenvironmental Engineering*; 131:598–609.

Gillis K., Dashti S., Hashash Y. 2015. Dynamic Calibration of Tactile Sensors for Measurement of Soil Pressures in Centrifuge. *ASTM Geotechnical Testing Journal*; 38(3),1–14.

Hushmand A., Dashti S., Davis C., Hushmand B., Zhang M., Ghayoomi M., McCartney J., Lee Y., Hu J. 2016a. Seismic Performance of Underground Reservoir Structures: Insight from Centrifuge Modeling on the Influence of Structure Stiffness. *Journal of Geotechnical and Geoenvironmental Engineering*, ASCE, 10.1061/(ASCE)GT.1943-5606.0001477.

Hushmand A., Dashti S., Davis C., Hushmand B., McCartney J., Hu J., Lee Y. 2016b. Seismic Performance of Underground Reservoir Structures: Insight from Centrifuge Modeling on the Influence of Backfill Soil Type and Geometry. *Journal of Geotechnical and Geoenvironmental Engineering*, ASCE 10.1061/(ASCE)GT.1943-5606.0001544, 04016058.

Hushmand, A., Dashti, S., Davis, C., McCartney, J.S., Hushmand, B. 2016c. A centrifuge study of the influence of site response, relative stiffness, and kinematic constraints on the seismic performance of buried reservoir structures. *Soil Dynamics and Earthquake Engineering*; 88: 427–438.

Idriss, I. M., and Sun, J. I. 1991. User's manual for SHAKE91, *Center for Geotechnical Modeling*, University of California, Davis, CA.

Ketcham, S. A., Ko, H. Y., and Sture, S. 1991. Performance of an earthquake motion simulator for a small geotechnical centrifuge. *Centrifuge 91*, H. Y. Ko and F. G. McLean, eds., Balkema, Rotterdam, The Netherlands, 361–368.

Kloukinas P., Langoussis M., Mylonakis, G. 2012. Simple wave solution for seismic earth pressures on non-yielding walls. *Journal of Geotechnical and Geoenvironmental Engineering*; 138(12), 1514–1519.

Mononobe N., Matsuo M. 1929. On the determination of earth pressures during earthquakes. *Proc. World Eng. Congr. Engineering Society of Japan*, Tokyo; 179–187.

Okabe S. 1924. General theory of earth pressure and seismic stability of retaining wall and dam. *Journal of Japan Society of Civil Engineers*; 12: 34–41.

Ostadan F. 2005. Seismic soil pressure for building walls – an updated approach. *Soil Dynamics and Earthquake Engineering*; 25: 785–793.

Papazafeiropoulos G., Psarropoulos P. N. 2010. Analytical evaluation of the dynamic distress of rigid fixed-base retaining systems. *Soil Dynamics and Earthquake Engineering*; 30 (12): 1417–1550.

Rovithis E.N., Parashakis H., Mylonakis G.E. 2011. 1D harmonic response of layered inhomogeneous soil: analytical investigation. *Soil Dynamics and Earthquake Engineering*; 31:879–890.

Seed H.G., Whitman RV. 1970. Design of earth retaining structures for dynamic loads. *ASCE Spec. Conf. Lateral Stress. Gr. Des. Earth Retaining Struct. American Society of Civil Engineers*, Reston, p. 103–147.

Veletsos A.S., Younan, A.H. 1994. Dynamic soil pressures on rigid retaining walls. *Earthquake Engineering and Structural Dynamics*; 23 (3), 275–301.

Vrettos C., Beskos D.E., Triantafyllidis T. 2016. Seismic pressures on rigid cantilever walls retaining elastic continuously non-homogeneous soil: An exact solution. *Soil Dynamics and Earthquake Engineering*; 82, 142–153.

Wagner, N., Sitar, N. 2016. On seismic response of stiff and flexible retaining structures. *Soil Dynamics and Earthquake Engineering*; 91, 284–293.

Wood, J.H. 1973. Earthquake induced soil pressures on structures. *Report No. EERL 73-05*, California Institute of Technology, Pasadena, CA.

Younan A.H., Veletsos A.S. 2000. Dynamic response of flexible retaining walls. *Earthquake Engineering and Structural Dynamics*; 29, 1815-1844.